Regular arrays of highly ordered ferroelectric polymer nanostructures for non-volatile low-voltage memories

Zhijun Hu[1,2], Mingwen Tian[3], Bernard Nysten[1,2] and Alain M. Jonas[1,2]*

Ferroelectric nanostructures are attracting tremendous interest because they offer a promising route to novel integrated electronic devices such as non-volatile memories and probe-based mass data storage. Here, we demonstrate that high-density arrays of nanostructures of a ferroelectric polymer can be easily fabricated by a simple nano-embossing protocol, with integration densities larger than 33 Gbits inch^{-2}. The orientation of the polarization axis, about which the dipole moment rotates, is simultaneously aligned in plane over the whole patterned region. Internal structural defects are significantly eliminated in the nanostructures. The improved crystal orientation and quality enable well-defined uniform switching behaviour from cell to cell. Each nanocell shows a narrow and almost ideal square-shaped hysteresis curve, with low energy losses and a coercive field of ~10 MV m^{-1}, well below previously reported bulk values. These results pave the way to the fabrication of soft plastic memories compatible with all-organic electronics and low-power information technology.

With increasing demand for miniaturization in microelectronics, ferroelectric nanostructures have attracted considerable practical[1,2] and theoretical[3,4] interest. It was shown for instance that ferroelectric properties exist in only a few monolayers of a ferroelectric polymer[5] or a few unit cells of complex ferroelectric oxides[6,7]. However, thinner films generally lead to degraded performance, with higher values of field being required to switch polarization and lower values of remnant polarization being attained[8]. These detrimental size effects are essentially caused by incomplete polarization screening at the surface and/or by structural defects introduced by the fabrication process[9]. The latter issue is even more severe for non-planar ferroelectric nanostructures such as nanowires and nanoparticles, because of their high surface-to-volume ratio[10]. So far, the fabrication of such one-dimensional or quasi-zero-dimensional nanostructures has mainly been achieved by scanning-beam lithography[11,12] or self-assembly[13–15] techniques. The former method may enable the fabrication of regular arrays of ferroelectric nanostructures, but the aggressive particle beams used in scanning-beam lithography severely damage the exposed surfaces of the nanostructures and deteriorate their ferro/piezoelectric performance. As for self-assembly methods, they enable high-throughput fabrication of ferroelectric objects tens of nanometres in lateral size and may improve crystal orientation and quality, but suffer from poor registration and limited control over feature size, which limits the practical interest of these systems.

Among ferroelectric materials, ferroelectric polymers are especially attractive as storage media for non-volatile memories, owing to their high flexibility, low cost, ease of production, stackability of a series of active memory layers and integrability with mainstream silicon technology and all-organic electronics[16,17]. Soft plastic non-volatile memories are currently the main bottleneck preventing the fabrication of all-organic flexible electronic systems, because organic transistors and displays have reached maturity and have entered the market. Poly(vinylidene fluoride-*ran*-trifluoroethylene) (P(VDF-TrFE)) is especially interesting for memory applications because it exhibits an excellent solution processability, a low processing temperature, excellent ferroelectric and electromechanical properties[18–20] and is already used for a variety of piezoelectric and pyroelectric devices[21] and organic thin-film transistors[17]. Still, the coercive field of P(VDF-TrFE) (~50 MV m^{-1}) is higher by an order of magnitude than typical values for ferroelectric oxide materials. Therefore, ferroelectric plastic memories require extremely thin films (<100 nm) to attain an operation voltage lower than 10 V (ref. 22), compatible with low-power technology and all-organic electronics. Unfortunately, decreasing the thickness below 100 nm also results in a decline of the ferroelectric switching performance, typified by a rapid increase of the coercive field, a lower remnant polarization and/or a longer switching time[22]. The declined performance has been mainly attributed to the reduction of crystallinity and/or crystallite size. By properly tuning the nature of the substrate, the decline of the performance can be limited; however, the coercive field still remains at about 50 MV m^{-1} (refs 22–24), much larger than typically found for inorganic ferroelectric oxides.

Here, we show that a rapid nano-embossing method can provide easy access to high-density arrays of ferroelectric polymer cells, while simultaneously controlling the orientation of crystallographic axes and the crystal quality within each nanocell (Fig. 1). The orientation of the chain axis (or *c* axis), which is the axis about which the dipole moment rotates on application of a vertical electric field, is uniformly aligned parallel to the substrate, thereby effectively easing the switching of the polarization. The preferential orientation of the crystals and the improvement of crystal quality in the ferroelectric nanocells guarantees a well-defined uniform operation of all nanocells in a given memory

---

[1]Unité de Physique et de Chimie des Hauts Polymères (POLY), Université catholique de Louvain, Place Croix du Sud 1, B-1348 Louvain-la-Neuve, Belgium, [2]Research Center in Micro- and Nanoscopic Materials and Electronic Devices, CeRMiN, Université catholique de Louvain, Place Croix du Sud 1, B-1348 Louvain-la-Neuve, Belgium, [3]NT-MDT Europe B. V., De Pinckart 54, 5674 CC, Nuenen, The Netherlands. *e-mail: alain.jonas@uclouvain.be.
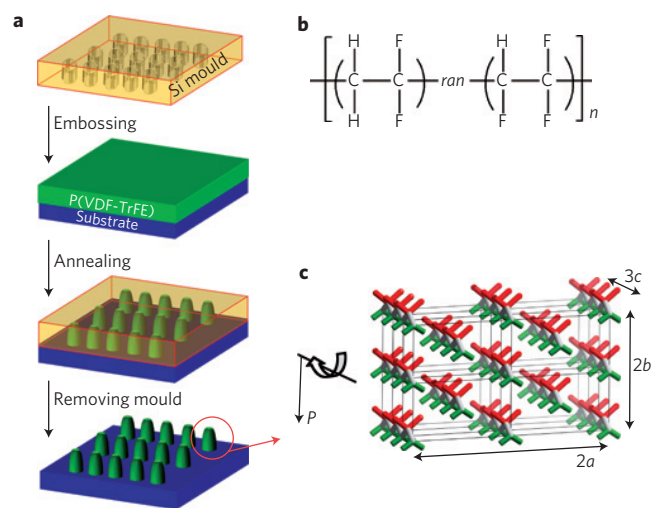
Figure 1 | Fabrication by nano-embossing of high-density arrays of crystalline nanostructures of a ferroelectric polymer. a, Schematic diagram of the nano-imprinting process. **b,** Chemical repeat unit of the P(VDF-TrFE) copolymer. **c,** Final orientation of the crystal unit cell of the P(VDF-TrFE) copolymer, after embossing but before poling, with a vertical polar b axis and in-plane a and c axes ($a = 0.905$ nm, $b = 0.512$ nm, $c = 0.255$ nm; red: F, green: H, grey: C) (ref. 35). This peculiar crystal setting favours the easy rotation of the dipole moment P about the chain axis on application of a vertical electric field.

device. In addition, ideal square-shaped and narrow hysteresis loops are achieved in the nanocells, with correspondingly low energy switching losses. Significantly, the coercive field of the highly ordered nanocells is decreased by a factor of 5 compared with that of polycrystalline thin films and bulk samples, thereby providing compatibility with low-voltage technologies such as complementary metal–oxide–semiconductor technology.

Nano-embossing or nano-imprint lithography is a rapid and low-cost lithographic technique that enables patterning of an initially flat thin film of soft molten material (mostly amorphous polymers)[25]. A priori, the nano-embossing technique could also be used to directly pattern semi-crystalline ferroelectric materials without generating structural defects, as the process only transfers molecules from one place to another. Actually, arrays of micrometre-sized ferroelectric polymer cells[26,27] or of Pb(Zr,Ti)O$_3$ sol–gel[28] (larger than 300 nm) protruding over a continuous thin film have already been obtained by embossing. However, no improvement of the ferroelectric properties was noted in these systems.

We speculated that this is because the size of the crystals in ferroelectric polymer materials is at least an order of magnitude smaller than the size of the patterned regions used in these previous studies[26–28], and because of the presence of a thick continuous residual film below the microstructures, resulting in the microscale ferroelectric cells achieved in these studies still containing many crystals of different orientation. Oriented and highly ordered nanostructures may however be obtained when crystallizing in complete confinement, that is, completely removing the residual film by pushing the nanostructured mould in contact with the silicon substrate, and decreasing the cavity size to well below the natural average distance between heterogeneous nucleation centres[29]. The elimination of the residual film is also advantageous for preventing cross-talking between different ferroelectric cells. In addition, nanoconfinement could also lead to preferred orientation by the grapho-epitaxial alignment of supramolecular assemblies such as crystals[29,30], or even by the molecular alignment of confined chains[31]. Preferential orientation could be advantageous

as ferroelectric properties are strongly anisotropic. Therefore, we significantly downscaled the size of the nanofeatures of embossing moulds to below the intrinsic size of the crystalline aggregates of the material. In addition, we designed the moulds in such a way as to ensure the total isolation of each polymer nanostructure during crystallization, thereby effectively preventing crystallization from propagating across different nanostructures. Hence, 50-nm-thick continuous thin films were prepared by spin-coating a P(VDF-TrFE) copolymer solution onto heavily n-doped (hence conducting) silicon wafers, most often covered by an amino-ended silane monolayer, which enhances the adhesion of the film on the substrate. The films were imprinted for 30 min at 140 °C in the liquid crystalline hexagonal phase of P(VDF-TrFE), which appears above its Curie temperature (118 °C) but below its melting temperature (150 °C), before being cooled to room temperature. The moulds were made of arrays of 100-nm-deep nanocavities having lateral dimensions in the same range. The much higher depth of the nanocavities compared with the film thickness effectively ensures that the mould contacts the substrate during imprinting (Fig. 1), resulting in the complete confinement of the polymer in the nanocavities, which is crucial for grapho-epitaxial alignment[29,32].

The surface of the nano-embossed film was imaged by atomic force microscopy (AFM, Fig. 2a,c) and transmission electron microscopy (TEM, Fig. 2e, inset), and shows a regular dense array of ferroelectric nanocells uniformly replicating the features of the mould. Given a period of 140 nm, the density of the array is at least 33 Gbits inch^{-2}. Corresponding images of the surface of a continuous thin film ($\sim$50 nm thick) similarly annealed in the absence of the mould are also provided in Fig. 2b,d,f for comparison. Consistent with previous work[33,34], the continuous film consists of randomly oriented grains with a large peak-to-valley roughness of $\sim$30 nm. At the surface of some grains, a threadlike fine texture with $\sim$10 nm period can be observed in the AFM phase image (arrows in Fig. 2d), probably due to the stacking of folded chain crystals in a grain[33]. In contrast, both the AFM phase image and the TEM image suggest the elimination of grain boundaries and of internal structural defects in each individual nanocell of the imprinted polymer.

The electron diffraction pattern of the continuous thin film (Fig. 2f) is composed of several diffraction rings, in agreement with the random orientation of the crystals in the film. However, only two diffraction rings are observed in the electron diffraction pattern of the P(VDF-TrFE) nanostructures obtained after the nano-embossing process (Fig. 2e), indicating preferential orientation. By circularly averaging the diffraction pictures (Fig. 2g), the presence of a weaker third reflection is also detected. Because two or more Bragg reflections may overlap in each diffraction ring, essentially owing to the pseudo-hexagonal nature of the crystal structure of the ferroelectric phase of P(VDF-TrFE) (Fig. 1c)[35], different crystal settings are compatible with the diffraction pattern of the nanostructures. To lift this uncertainty, the samples were studied by Fourier-transform infrared reflection–absorption microspectroscopy (Fig. 2h). One of the conditions for the appearance of an infrared band is that its transition dipole moment possesses a component parallel to the electric field. For our reflection geometry, the electric field is parallel to the plane of the substrate. The 1,288 cm^{-1} A$_1$ band (symmetric stretching vibration of CF$_2$), which has a transition dipole moment μ_b parallel to the polar b axis[33], is practically extinct in the nano-embossed film, which indicates that the b axis is strongly tilted away from the substrate in the nano-imprinted film. In contrast, the 1,400 cm^{-1} B$_1$ band (wagging vibration of CH$_2$, μ_c parallel to the chain c axis) and the 1,187 cm^{-1} B$_2$ band (antisymmetric stretching and rocking vibration of CF$_2$, μ_a parallel to the a axis) appear prominently in the nano-imprinted film, indicating an in-plane orientation of the a and c axes.
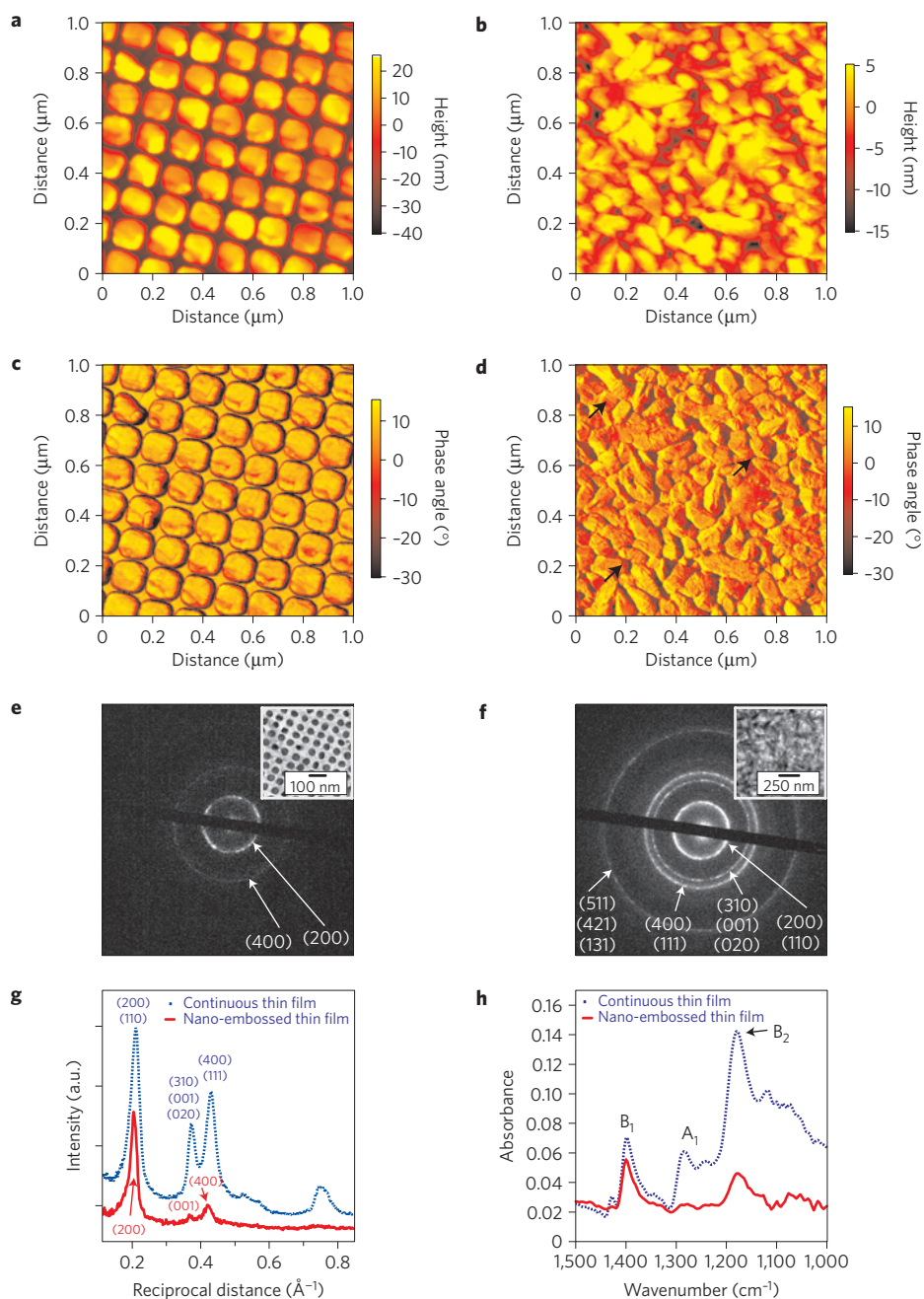
Figure 2 | Microstructure of nano-imprinted P(VDF-TrFE). Comparison of the structure of an array of nano-imprinted nanostructures (left column, or solid lines in **g,h**) and of a similarly annealed continuous copolymer film (right column, or dotted lines in **g,h**). **a,b**, AFM topography images, showing that a high density of nanostructures can be obtained by the process. **c,d**, AFM phase images, illustrating the much more defective microstructure of the continuous film. Arrows indicate stacks of folded-chain lamellae in the continuous film. **e,f**, Electron diffraction patterns and corresponding TEM images (insets) of the nanostructures and of the continuous film. The numerous rings of the continuous film indicate a random orientation of the crystals in the film; in contrast, the diffraction pattern of the nanostructures is compatible with a vertical orientation of the polar b axis and an in-plane orientation of the a and c axes. **g**, Circular averages of the electron diffraction patterns of **e** (nanostructures, solid line) and **f** (continuous film, dotted line). **h**, Infrared reflection microspectroscopy of the nanostructures (solid line) and of a continuous film (dotted line). The dichroism exhibited by the nanostructures is in complete agreement with the electron diffraction pattern and the crystal setting shown in Fig. 1c.

With this information, the electron diffraction pattern of the nanostructures can then be safely indexed as shown in Fig. 2e,g, corresponding to a setting of the crystal where the polar b axis is vertical, and the a and c axes are in the plane of the substrate (Fig. 1c). This specific preferential orientation is crucial for applications, because the ferroelectric dipole moment of the polymer can now easily rotate about the horizontal chain c axis on application of a vertical electric field as shown in Fig. 1, and because

the remnant polarization will be maximized owing to the vertical orientation of the polar b axis.

The preferred orientation of the chain c axis and the perfection of the crystals in the nanocells do indeed translate into favourable ferroelectric properties in the direction perpendicular to the substrate. Figure 3 shows the piezoresponse amplitude and phase images of the nano-embossed thin films measured by vertical piezoresponse force microscopy (PFM), where the piezoresponse
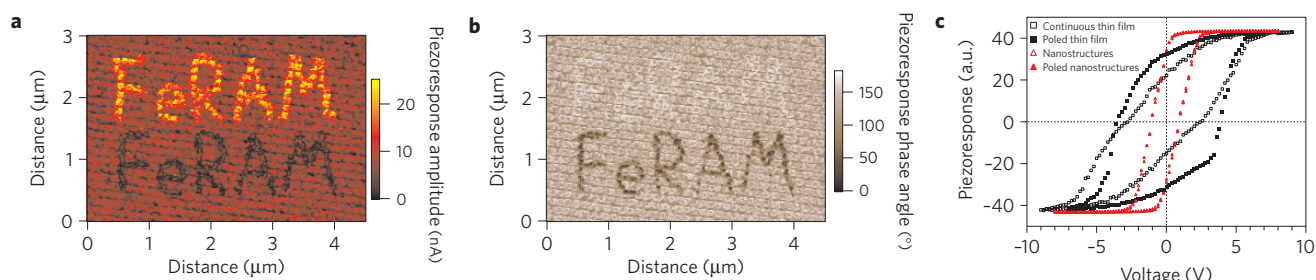
Figure 3 | Ferroelectric properties of the P(VDF-TrFE) nanostructures. a,b, PFM piezoresponse amplitude (**a**) and piezoresponse phase (**b**) of an array of nanostructures. The uniform background corresponds to unpoled nanostructures. The bright letters in **a** were polarized with a positive d.c. voltage (+5 V), whereas the dark letters were polarized with a negative d.c. voltage (−5 V) before imaging. **c**, PHLs of unpoled nano-embossed nanostructures (open triangles), of an unpoled similarly annealed P(VDF-TrFE) thin film (open squares) and of the poled nanostructures (filled triangles) and film (filled squares). The coercive voltage and power losses are significantly reduced by the improvement of the crystal quality and orientation of the nanostructures.

amplitude and phase provide information on the electromechanical coefficient (proportional to the local polarization) and on the direction of the local polarization, respectively[36]. The piezoresponse amplitude and phase in each nanocell is uniform in colour over the unpoled nano-embossed regions (background of the letters in Fig. 3), showing the homogeneity of the dipole moment and of the orientation of the polar *b* axis in each P(VDF-TrFE) nanocell before poling. Each nanocell is thus composed of a monodomain, and all nanocells are equivalent. The homogeneity of the ferroelectric properties in the nanocells enables a uniform switching behaviour from cell to cell at the nanometre scale. For example, information can be written in the nano-embossed thin films by applying small d.c. voltages to the conducting tip of an AFM run in the nanolithography mode. In the piezoresponse amplitude image shown in Fig. 3a, the bright nanocells were poled with a positive bias (5 V) before being imaged by PFM, whereas the dark nanocells were poled with a negative bias. The piezoresponse amplitude is enhanced by poling with a downward electric field compared with the initially formed nanocells. This indicates that the total dipole moment of P(VDF-TrFE) crystals tilts even more perpendicularly to the substrate after the application of the electric field. However, the phase shift (Fig. 3b) in the corresponding region remains essentially unchanged, showing that the globally vertical orientation of the dipole moments is not changed when poling with a downward electric field: the electronegative CF_2 groups in the bulk of the nanostructures remain pointing towards the free surface of the nanocells. This supports the notion that the total dipole moment was not completely vertically aligned in the nanostructures before poling, probably because of the contributions of more disordered regions such as interfaces where the *b* axis may be not vertical after imprinting. Logically, when the nanocells are polarized with an upward electric field (black letters in Fig. 3a,b), the dipole moment is completely reversed, exhibiting a decreased piezoresponse amplitude and a reversed phase shift. The region shown in Fig. 3a,b was measured again by PFM one day after poling; the images were found to be virtually identical to the initial ones, showing the good stability of the orientation.

The piezoresponse hysteresis loops (PHLs) of the nanocells were also measured by PFM. These loops reflect the switching of the dipole moment averaged over the region beneath the conducting tip, from which phenomenological characteristics such as coercive voltage and work of switching can be obtained[37], on the basis of the current understanding of switching under PFM conditions. The PHLs of the unpoled nanocells and of the similarly annealed unpoled thin films (Fig. 3c) are symmetric, indicating a minimal influence of the substrate. More importantly, the shapes of the PHLs in the first run before poling are very different, with nanocells showing an almost ideal square shape with a coercive voltage of

±0.8 V and a sharp saturation at ±2.6 V, whereas the similarly annealed continuous film shows a skewed hysteresis curve with a coercive voltage of about ±2.5–2.8 V and a gradual saturation at about ±7.0 V. After poling the samples with an upward or downward electric field (5 V voltage), the PHLs of the nanocells exhibit traces identical to the ones obtained before poling, which confirms that the crystals in the nanocells were already of high preferred orientation and quality before poling. In stark contrast, the shape and characteristic of the PHLs of the continuous film are strongly changed after the poling process (Fig. 3c, filled squares): the PHLs of the poled thin film change from a skewed to a quasi-squared shape, with an improved piezoresponse amplitude at zero field but also an increased coercive voltage. In addition, the piezoresponse amplitude, that is, the remnant polarization, of the unpoled nanocells equals the one of the poled thin films, indicating again the preferred orientation of crystals and domains in the nanostructures obtained just after embossing. Another striking difference between the unpoled thin film and the nanostructures is the slope of the PHLs, which is much steeper for the nanostructures, and identical to the one found after poling the film. Again, this supports the notion of a high preferential orientation pre-existing in the unpoled nanostructures.

From these PHLs, the coercive field can be estimated to be 10 MV m^{-1} for the nanocells that are of ~80 nm thickness (~50 nm before embossing), which is a factor of 5 lower than the one of the similarly annealed unpoled 50-nm-thick continuous film (~50 MV m^{-1}) and a factor of 7 lower than the poled continuous film (~75 MV m^{-1}). It should be noted that the PHLs of P(VDF-TrFE) with similar compositions have also been measured[38] for ultra-thin polycrystalline films prepared by the Langmuir–Blodgett method. The coercive field in a 64-nm-thick Langmuir–Blodgett film was about 180 MV m^{-1} from PFM, much larger than the values achieved here.

Polarization reversal in ferroelectric polymers is carried out by 180° rotation of dipole moments about the chain axis. The flipping of the –CF$_2$– groups around the chain axis can occur once the electric field is larger than the energy barrier for dipole rotation. It was established by scanning tunnelling microscopy[39] that a tip bias of ±0.57 V is needed to completely trigger the flipping of the –CF$_2$– groups around the chain axis in a two-dimensional surface lattice structure of P(VDF-TrFE). In our case, the coercive voltage (±0.8 V) of the nanocells is very close to this ultimate threshold voltage for dipole rotation, which indicates that the chains rotate almost as easily in our systems as in a 2D lattice.

There are two reasons for the observed decrease of the coercive field after nano-embossing. The first one is the favourable orientation of the *c* axis, which enables an optimal coupling between the electric field and the dipole moment. The second is the improvement of crystal quality in the nano-embossed

film. According to the classical domain nucleation and growth mechanism, reversed domains nucleate beneath the electrode under an applied voltage, then elongate in the direction parallel to the electric field and simultaneously in the lateral direction until they reach an equilibrium size or meet a pinning point. Therefore, grain boundaries and internal structural defects in the crystals strongly influence polarization switching. The easy switching of polarization of the nano-embossed film thus points to a much decreased defect density, as already mentioned on the basis of the inspection of AFM images. In the thermodynamic limit where the pinning effects can be neglected, the coercive voltage V_c is solely determined by the domain wall energy σ_{wall} and by the spontaneous polarization P_s (ref. 37), $V_c = 5\beta\sigma_{wall}\pi^2/8P_s$, where β is a proportionality coefficient of the order of unity. Taking $P_s = 0.087\,\mathrm{C\,m^{-2}}$ (ref. 40), the domain wall energy can thus be estimated as $11.3\,\mathrm{mJ\,m^{-2}}$ (using $\beta = 1$ and a coercive voltage of 0.8 V), which is of the same order as found for $BaTiO_3$ ($\sigma_{wall} = 7$–$15\,\mathrm{mJ\,m^{-2}}$) (refs 37,41) but an order of magnitude lower than reported for $PbTiO_3$ ($\sigma_{wall} = 169\,\mathrm{mJ\,m^{-2}}$) (ref. 42). This is in good agreement with the notion that pinning defects are indeed practically excluded from the nanocells. Note that the preferential orientation of the chain axis and the elimination of structural defects in the nanocells also reduce the energy loss during the polarization switching. The energy loss can be estimated from the area within the hysteresis loops[37], and it is obviously much smaller for the nanocells than for the similarly annealed thin film (Fig. 3c).

Summing up, nano-imprinting of ferroelectric polymers offers exciting opportunities for the fabrication of high-density non-volatile ferroelectric memories of low writing voltage. Our results show that, by using properly designed moulds, it is possible to orient the crystals of ferroelectric polymers while simultaneously patterning them. This translates into low-voltage operation and uniform switching from cell to cell, which should now enable ferroelectric polymer memories to compete against more expensive technologies such as flash memories. In the future, the complete integration of the memory arrays with printed plastic electrodes should lead to cheap all-plastic high-density flexible memories, which will integrate seamlessly with current polymer electronic devices such as displays and transistors. Alternatively, the ferroelectric nanostructures could also be directly integrated in the gate stack of a field-effect transistor, as their low-voltage operation is compatible with the requirements of complementary metal–oxide–semiconductor technology. Significantly, the tuning of chain or crystal orientation by nano-imprinting holds promise for other materials and in other fields as well, such as sol–gel processing of ferroelectric precursors, phase-change or organic memories, magnetic storage media, multiferroic systems and other types of nanodevice.

Methods

Materials and methods. The P(VDF-TrFE) 70/30 mol% copolymer was obtained from Solvay SA and used as-received. The P(VDF-TrFE) powder was dissolved in N,N-dimethylformamide at a concentration of 1.5% w/v. Thin films were prepared by spin-coating in a class 1,000 clean room environment, then dried in a vacuum oven at room temperature for 24 hours. The film thickness was controlled by varying the spin speed, measured by ellipsometry using 1.4 as the index of refraction, and confirmed by AFM. The substrates used were highly doped silicon wafers with or without a 300-nm-thick layer of thermally grown silicon oxide, cleaned in freshly prepared piranha solution (H_2O_2 (27%) and H_2SO_4 (98%) 1:1). To enhance the adhesion of P(VDF-TrFE) to the substrate, the surface of the silicon wafer was modified by immersing the substrate in a 0.1 M solution of amino-propyl-silane in dry acetone at 60 °C for 20 min in a glove box. The silicon moulds were prepared by electron beam lithography and reactive ion etching. The nanocavities on the mould cover an area of $100 \times 100\,\mu m^2$. To facilitate mould separation after embossing, the moulds were coated with a monolayer of perfluorodecyltricholosilane deposited from the gas phase. The height of the protrusions was 100 nm, as determined by the thickness of the thermal silicon oxide grown on the mould before lithography to define the etching depth.

Nanostructure fabrication. The nano-embossing experiments were carried out with an Obducat 3-inch nano-imprinter in a class 1,000 clean room environment. A pressure of 60 bars was applied to the silicon mould ($1.0 \times 1.0\,cm^2$). The system was cooled with a nitrogen gas flow. The print mould was pressed against the polymer film under pressure at 140 °C and held for 30 min to partially relax the strains induced by the flow and to increase crystallinity. After cooling the system to room temperature, we removed the mould from the samples for examination.

Morphology and structure characterization. The surface of the continuous thin films and arrays of nanocells was imaged in intermittent contact mode with a Veeco Nanoscope IV Multimode AFM, using Si cantilevers ($7.4\,N\,m^{-1}$ force constant at a nominal frequency of 160 kHz, from Nanosensors). TEM (Zeiss Leo922 operated at 120 keV) was used to investigate the morphology and structure of the continuous thin films and of the nanocells. Silicon wafers with a 300-nm-thick silicon oxide layer were used as substrates for this purpose. After embossing, a thin carbon film was evaporated onto the surface of the samples for mechanical reinforcement and charge conduction. For the nanostructured samples, the carbon film also served as a glue preventing the disintegration of the nano-imprinted film during the floating-off process. The continuous polymer thin films or nanocells were subsequently floated over a diluted HF solution, and were collected on TEM copper grids. As P(VDF-TrFE) is very sensitive to electron beam exposure, a very low dose of electrons was used to obtain the electron diffraction patterns.

Fourier-transform infrared microspectroscopy was carried out on a Continuμm microscope (Nicolet) under reflection mode. The aperture size, which is used to define the infrared beam area, is 200 μm. All spectra were averages of 128 scans with $8\,cm^{-1}$ resolution.

Ferro/piezoelectric properties. A commercial scanning probe microscope (NTEGRA Prima from NT-MDT) was used for PFM measurements. Imaging and poling of ferroelectric domains were carried out at room temperature using a conductive Pt-coated Si cantilever ($5\,N\,m^{-1}$ force constant, MikroMasch, used at a frequency of 150 kHz). The topography, magnitude and phase shifts of the cantilever resonance were acquired simultaneously using an a.c. modulation voltage of 2 V (point to point) at the shoulder of the contact resonance. The magnitude of the cantilever resonance reflects the local electromechanical response of the sample surface during application of the a.c. voltage to the tip. The phase yields information on the direction of polarization below the tip.

Local poling of the continuous thin films and of nanocells was carried out by using the conductive tip as the top electrode. A pattern composed of vector lines is drawn in the controlling software and then scanning is carried out over a square region. A pulsed (0.1 ms dwell time) d.c. bias ($\pm5\,V$) is applied at the predetermined positions drawn in the controlling software.

Hysteresis loops of individual nanocells or of the continuous thin films were recorded by positioning the tip on top of a selected nanocell or over a position in the continuous thin films, and monitoring the piezoresponse signal as a function of the d.c. bias applied to the tip. The d.c. bias was swept by 0.2 V increments.

References

1. Scott, J. F. Applications of modern ferroelectrics. *Science* **315**, 954–959 (2007).
2. Ahn, C. H., Rabe, K. M. & Triscone, J.-M. Ferroelectricity at the nanoscale: Local polarization in oxide thin films and heterostructures. *Science* **303**, 488–491 (2004).
3. Junquera, J. & Ghosez, P. Critical thickness for ferroelectricity in perovskite ultrathin films. *Nature* **422**, 506–509 (2003).
4. Naumov, I. I., Bellaiche, L. & Fu, H. Unusual phase transitions in ferroelectric nanodisks and nanorods. *Nature* **432**, 737–740 (2004).
5. Bune, A. V. *et al.* Two-dimensional ferroelectric films. *Nature* **391**, 874–877 (1998).
6. Fong, D. D. *et al.* Ferroelectricity in ultrathin perovskite films. *Science* **304**, 1650–1653 (2004).
7. Lichtensteiger, C., Triscone, J.-M., Junquera, J. & Ghosez, P. Ferroelectricity and tetragonality in ultrathin $PbTiO_3$ films. *Phys. Rev. Lett.* **94**, 047603 (2005).
8. Rabe, K. M., Ahn, C. H. & Triscone, J.-M. *Physics of Ferroelectrics: A Modern Perspective* (Springer, 2007).
9. Gruverman, A. & Kholkin, A. Nanoscale ferroelectrics: Processing, characterization and future trends. *Rep. Prog. Phys.* **69**, 2443–2474 (2006).
10. Schilling, A., Bowman, R. M., Catalan, G., Scott, J. F. & Gregg, J. M. Morphological control of polar orientation in single-crystal ferroelectric nanowires. *Nano Lett.* **7**, 3787–3791 (2007).
11. Alexe, M., Harnagea, C., Hesse, D. & Gösele, U. Patterning and switching of nanosize ferroelectric memory cells. *Appl. Phys. Lett.* **75**, 1793–1795 (1999).
12. Ganpule, C. S. *et al.* Scaling of ferroelectric and piezoelectric properties in $Pt/SrBi_2Ta_2O_9/Pt$. *Appl. Phys. Lett.* **75**, 3874–3876 (1999).
13. Alexe, M. *et al.* Switching properties of self-assembled ferroelectric memory cells. *Appl. Phys. Lett.* **75**, 1158–1160 (1999).

14. Dawber, M., Szafraniak, I., Alexe, M. & Scott, J. F. Self-patterning of arrays of ferroelectric capacitors: Description by theory of substrate mediated strain interactions. *J. Phys. Condens. Matter.* **15**, L667–L671 (2003).

15. Bai, M. & Ducharme, S. Ferroelectric nanomesa formation from polymer Langmuir–Blodgett films. *Appl. Phys. Lett.* **85**, 3528–3530 (2004).

16. Malin, L., Stolichnov, I. & Setter, N. Ferroelectric polymer gate on AlGaN/GaN heterostructures. *J. Appl. Phys.* **102**, 114101 (2007).

17. Naber, R. C. *et al.* High-performance solution-processed polymer ferroelectric field-effect transistors. *Nature Mater.* **4**, 243–248 (2005).

18. Furukawa, T. Ferroelectric properties of vinylidene fluoride copolymers. *Phase Transit.* **18**, 143–211 (1989).

19. Tashiro, K. & Kobayashi, M. Structural study of the ferroelectric phase transition of vinylidene fluoride-trifluoroethylene copolymers: 4. Poling effect on structure and phase transition. *Polymer* **27**, 667–676 (1986).

20. Baltá Calleja, F. J. *et al.* Structure and properties of ferroelectric copolymers of poly(vinylidene fluoride). *Adv. Polym. Sci.* **108**, 1–48 (1993).

21. Lovinger, A. J. Ferroelectric polymers. *Science* **220**, 1115–1121 (1983).

22. Naber, R. C., Blom, P. W., Marsman, A. W. & de Leeuw, D. M. Low voltage switching of a spin cast ferroelectric polymer. *Appl. Phys. Lett.* **85**, 2032–2034 (2004).

23. Xu, H., Zhong, J., Liu, X., Chen, J. & Shen, D. Ferroelectric and switching behavior of poly(vinylidene fluoride-trifluoroethylene) copolymer ultrathin films with polypyrrole interface. *Appl. Phys. Lett.* **90**, 092903 (2007).

24. Gerber, A. *et al.* Low-voltage operation of metal-ferroelectric-insulator-semiconductor diodes incorporating a ferroelectric polyvinylidene fluoride copolymer Langmuir–Blodgett film. *J. Appl. Phys.* **100**, 024110 (2006).

25. Chou, S. Y., Krauss, P. R. & Renstrom, P. J. Imprint lithography with 25-nanometer resolution. *Science* **272**, 85–87 (1996).

26. Zhang, L., Ducharme, S. & Li, J. Microimprinting and ferroelectric properties of poly(vinylidene fluoride-trifluoroethylene) copolymer films. *Appl. Phys. Lett.* **91**, 172906 (2007).

27. Kang, S. J. *et al.* Localized pressure-induced ferroelectric pattern arrays of semicrystalline poly(vinylidene fluoride) by microimprinting. *Adv. Mater.* **19**, 581–586 (2007).

28. Harnagea, C. *et al.* Mesoscopic ferroelectric cell arrays prepared by imprint lithography. *Appl. Phys. Lett.* **83**, 1827–1829 (2003).

29. Hu, Z., Baralia, G., Bayot, V., Gohy, J.-F. & Jonas, A. M. Nanoscale control of polymer crystallization by nanoimprint lithography. *Nano Lett.* **5**, 1738–1743 (2005).

30. Givargizov, E. I. in *Handbook of Crystal Growth* Vol. 3: Thin Films and Epitaxy (ed. Hurle, D. T. J.) (Elsevier Science, 1994).

31. Nguyen, T.-Q., Wu, J., Doan, V., Schwartz, B. J. & Tolbert, S. H. Control of energy transfer in oriented conjugated polymer-mesoporous silica composites. *Science* **288**, 652–656 (2000).

32. Hu, Z. *et al.* High-throughput fabrication of organic nanowire devices with preferential internal alignment and improved performance. *Nano Lett.* **7**, 3639—3644 (2007).

33. Park, Y. J. *et al.* Molecular and crystalline microstructure of ferroelectric poly(vinylidene fluoride-co-trifluoroethylene) ultrathin films on bare and self-assembled monolayer-modified Au substrates. *Macromolecules* **41**, 109–119 (2008).

34. Kimura, K. *et al.* Orientation control of ferroelectric polymer molecules using contact-mode AFM. *Eur. Polym. J.* **40**, 933–938 (2004).

35. Bellet-Amalric, E. & Legrand, J. F. Crystalline structures and phase transition of the ferroelectric P(VDF-TrFE) copolymers, a neutron diffraction study. *Eur. Phys. J. B* **3**, 225–236 (1998).

36. Kholkin, A. L., Kalinin, S. V., Roelofs, A. & Gruverman, A. in *Scanning Probe Microscopy: Electrical and Electromechanical Phenomena at the Nanoscale* (eds Kalinin, S. V. & Gruverman, A.) (Springer, 2007).

37. Jesse, S., Baddorf, A. P. & Kalinin, S. V. Switching spectroscopy piezoresponse force microscopy of ferroelectric materials. *Appl. Phys. Lett.* **88**, 062908 (2006).

38. Bystrov, V. S. *et al.* Nanoscale polarization patterning of ferroelectric Langmuir–Blodgett P(VDF-TrFE) films. *J. Phys. D: Appl. Phys.* **40**, 4571–4577 (2007).

39. Cai, L. *et al.* Surface structure of ultrathin copolymer films of ferroelectric vinylidene fluoride (70%) with trifluoroethylene (30%) on graphite. *Phys. Rev. B* **70**, 155411 (2004).

40. Duan, C.-G. *et al.* Simulations of ferroelectric polymer film polarization: The role of dipole interactions. *Phys. Rev. B* **69**, 235106 (2004).

41. Padilla, J., Zhong, W. & Vanderbilt, D. First-principles investigation of 180° domain walls in $BaTiO_3$. *Phys. Rev. B* **53**, R5969–R5973 (1996).

42. Meyer, B. & Vanderbilt, D. *Ab initio* study of ferroelectric domain walls in $PbTiO_3$. *Phys. Rev. B* **65**, 104111 (2002).

Acknowledgements

Author contributions

Z.H. designed and carried out the experiments, participated in the data analysis and wrote the paper. M.T. provided support for the PFM measurements. B.N. provided support for the interpretation of AFM experiments. A.M.J. planned the project, contributed to the experiment design and data analysis, and wrote the paper.

Additional information